The Sinkhole Hazard Study at Casalabate (Lecce, Italy) using Geophysical and Geological Surveys

Leucci G.[1], De Giorgi L.[2], Delle Rose M.[3]

[1]Istituto di Scienze dell'Atmosfera e del Clima – CNR, Lecce, Italy
[2]Istituto per i Beni Archeologici e Monumentali – CNR, Lecce, Italy

Abstract— *In the last two decades the village of Casalabate was affected by a number of sinkhole events, the last episode occurring on 7 January 2012. Due to some geological and geotechnical uncertainties, Casalabate became an intriguing case study of sinkhole hazard in urban areas and three geological-geophysical models were recently proposed by three different studies. In this paper new geophysical data and some epistemological consideration were done. The results are a contribution to an efficient predictive model that could be well define both the geological setting and sinkhole hazard.*

Keywords— urban environment, sinkhole geohazard, electrical resistivity tomography, ground penetrating radar, karst coastal plane; new data

I. INTRODUCTION

Casalabate is a coastal small town frequently affected by sinkhole events. The first noticed event occurred on 1993 and caused several destructions of buildings. In the same year, a sinking of a small portion of emerged beach happened (Delle Rose and Federico, 2002). Four years later a collapse affected the submerged portion of beach and allowed the formations of a submarine spring, since then the bathing was forbidden for some weeks. Two episodes of sinkhole on the emerged beach occurred during 2000 and 2004, along a strike no longer than 30 meters. Each of these caused on surface short-lived elliptical depression quickly filled by sand. All the aforementioned episodes occurred inside a narrow area (about 250 m long and 100 m wide) close to the coast and oriented according to a north-north-east - south-south-west tectonic structures system (Delle Rose and Leucci, 2010). Further episodes occurred on March 2010, November 2010 and March 2011. The last noticed sinkhole happened on 7 January 2012. Usually the sinkholes occurred during or after rains or sea storms and each episode lasts some minutes at least. Due to geological and geotechnical uncertainties, Casalabate became an intriguing case study of sinkhole hazard in urban areas and three geological-geophysical models were recently proposed to explain the ground-instability and to asses the related hazard (Delle Rose and Leucci, 2010; Calò et al., 2011; Margiotta et al., 2012). 3D geological model and new geophysical data here shown can contribute to an efficient predictive model taking into account the hydrogeology context. Moreover, some epistemological considerations had performed to improve the interdisciplinary exchange between geologists and geophysicists.

II. GEOLOGICAL SETTING

Casalabate is located on the Adriatic side of the Salento Peninsula (Southern Italy) on a coastal plain elevated a few meters above sea level (Fig. 1). The Salento Peninsula is the emerged southeastern portion of the Adriatic Carbonatic Plate (Auct.) which is formed by Jurassic-Cretaceous limestones and dolostones covered by Tertiary and Quaternary carbonates and marls. The bedrock of Casalabate is build up by Quaternary carbonate deposits, some tens of meters thick, lie on Cretaceous limestone (Rossi, 1969). Nevertheless, geological and geotechnical data suitable for civil engineering lacked until few years ago. As a consequence, to face the sinkhole hazard the municipal authority performed an extensive bedrock survey by means of boreholes and geophysical measures. The results of such a survey were used in Delle Rose and Leucci (2010) and in Calò et al. (2011). Casalabate bedrock resulted built up by "two overlap units". The lower of which is a moderately cemented massive calcarenite made up mainly of marine bioclasts and medium-large in grain size. The upper units is formed by sets of variableness cemented thinly laminated and cross-stratified calcarenite [ancient dunes] whose grains were terrestrial or marine supplied. The latter is 5-10 m thick, whereas the base of the former are locally unknown but, on the base of the setting surrounding Casalabate, the thickness of the massive calcarenite doesn't excess 20-25 m. Both the calcarenite units show a nearly omogeneous low-angle beds dip, which seems to be due to primary clinostratification as well as tectonic eastward tilting" (Delle Rose and Leucci, 2010). Four tectonic fracture systems (medium strikes N 5°E, N55°E, N100°E and N145°E) probably affect both the stratigraphic units. The shape and orientation of the landforms are clearly due to the spatial arrangement of the tectonic fractures. This structural control is particularly evident as it concerns the shape of the depressions

filled by clayey-silt marsh deposits. The calcarenite units were interested by various periods of dissolution karst processes to begin from the Middle Pleistocene. Usually such processes are named as "parakarstic" (Auct.) to emphasize the small dimension of the morphological forms respect those charactering the Jurassic-Cretaceous limestones and dolostones.

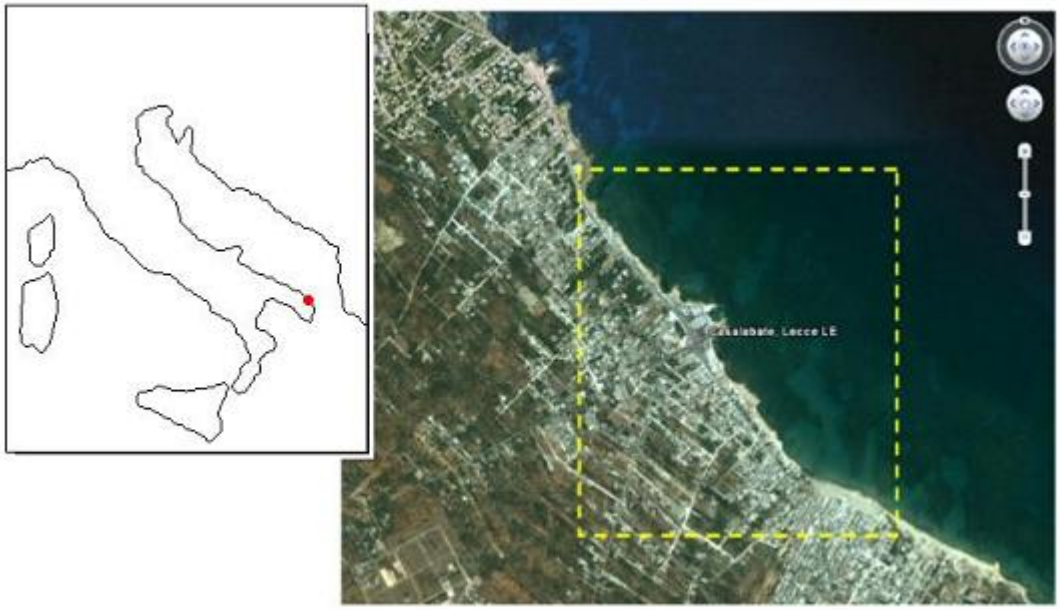

FIG. 1 – SURVEYED AREA (PHOTO BY GOOGLE EARTH)

A shallow coastal aquifer flows out along the Casalabate coast. The groundwater circulation is influenced by the tectonic fracture systems and is manifested by some submarine springs. Underwater investigations of the sinking of a portion of submerged beach in 1997 revealed the presence of a karst spring (Delle Rose and Federico, 2002) probably joined with the cave that induced the 1993 sinkholes. Such springs are not perennial and can occur suddenly. The last case of new spring formation occurred below an house on the beginning of September 2013 and caused a new warning to the residents.

III. 3D GEOLOGICAL MODEL

Using the software Groundwater Modeling System (GMS), a 3D geological model and a 3D groundwater model are in progress. The scope of building the models is to simplify the field problem and organize the field data so that the system can be analyzed more readily (Anderson and Woessner, 2002). The conceptualization of the models includes synthesis and framing up of data pertaining to geology, hydrogeology, hydrology, and meteorology. The lithologic data were collected from 23 core lithologs data (kindly provided by the technical office of Lecce municipality). Such a borehole survey was performed on 2008 and was related to the project "actions to protect the soil in the hydrogeological risk areas of the municipality of Lecce" funded by the Ministry of Environment and Protection of Land.

The geological model was created using a block-centric finite-difference grid. The gridding was performed through the eight nearest-neighbor methodology with 3-D interpolation by average minimum distance. The solid model was developed to a depth of about 10 m below the ground level. The sensitivity of the model was tested by varying the horizontal and vertical spacing of the nodes, and an optimized final model, least sensitive to changes in spatial resolution (i.e., smaller grid sizes), was built. The resolution of the final model was 100m×100m×2m. The resulting discretization consisted of 250nodes×250nodes×100nodes, obtaining 6,250,000 solid model nodes, each with a voxel volume of 20,000 m^3. It should be noticed that the results of the modeling are not free from uncertainties, which could be reduced by increasing data points, but they illustrate one of the most probable scenarios. The smallest scale of variation that the model is able to depict is equal to the resolution of one voxel. The 3D geological model (Fig. 2a) with the cross-sections in Fig. 2b provides a depictions of the bedrock of the studied area. Such model was vertically discretized in 8 layers (paving; artificial landfills; sands of beach; organic soils; residual soils; marsh deposits; cemented thinly laminated and cross-stratified calcarenites; moderately cemented massive calcarenites). The layers were allowed to have seepage from the top and leakage through the base, making them hydraulically connected. The top-most layer and the second layer were defined as unconfined. The rest of the layers were defined as confined, as the water table was not expected to fall >10 m. Such a model has reached a first level of

advancement and needs several new data to be fully efficient, to start from the boundary conditions as well as the real physical characters of the higher layers.

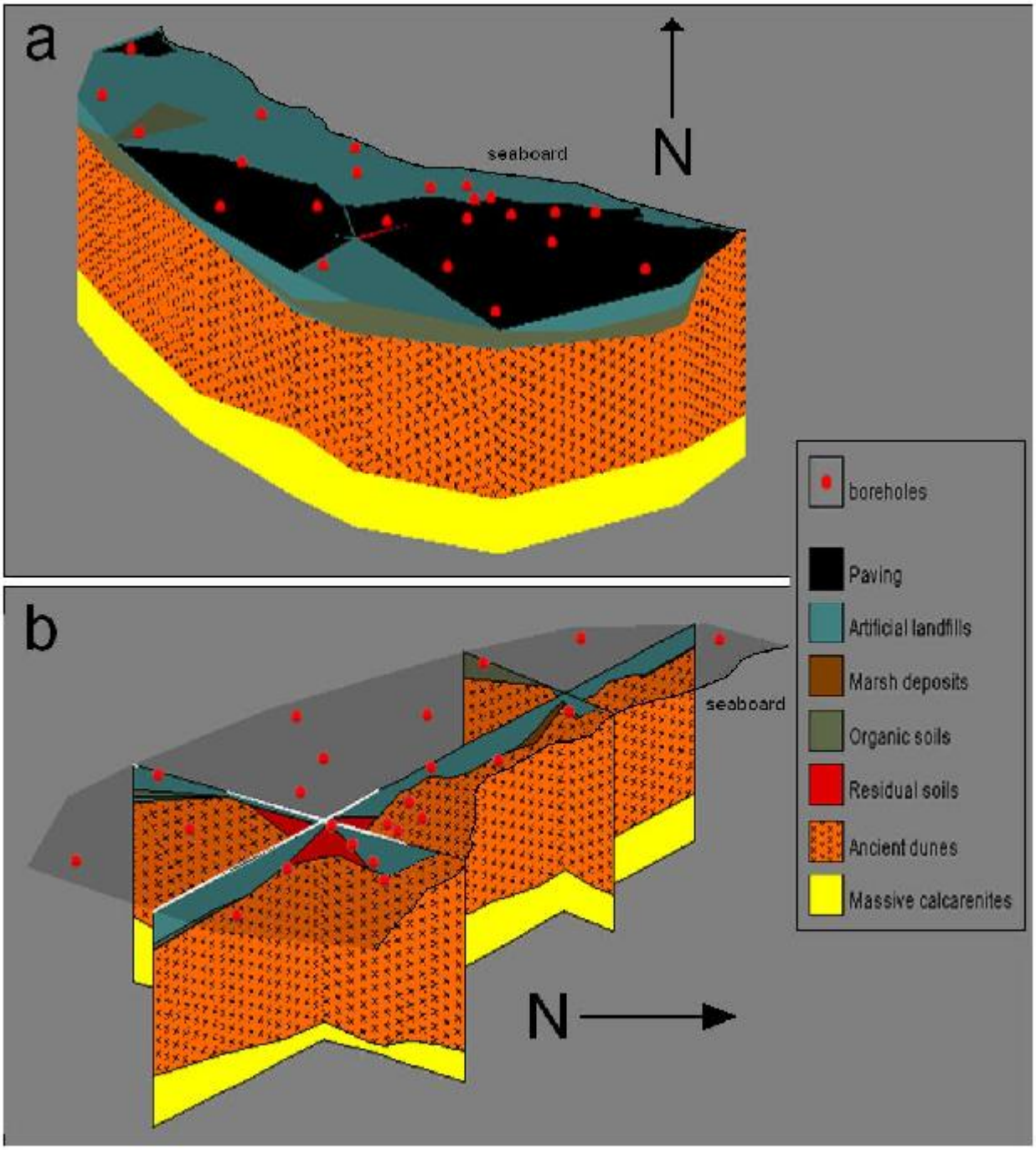

FIG. 2 – 3D GEOLOGICAL MODEL (A) AND CROSS SECTIONS OF CASALABATE URBAN AREA (B)

Given the heterogeneity and complexity associated with the study area (e.g. local-scale variations of aquifer properties), some generalizations, simplifications and assumptions will be made to construct the groundwater flow model. The modeling area is limited in the east by the Adriatic sea, and it accounts for about 1,5 km in length and 0,5 km in width. The 3-D constant-density groundwater flow will be simulated by a block-centric, finite-difference grid model, using MODFLOW code inside GSM software. Furthermore MODAEM code, which allows the analysis to the analytical elements (polygons, lines and points), will be used.

IV. NEW GEOPHYSICAL MEASUREMENTS

In our previous work, we have proposed a method to integrate geophysical survey and geological knowledge to characterize

the sinkhole hazard at Casalabate. As regards geophysics work, the performed 3D Ground Penetrating Radar (GPR) and 3D Electrical Resistivity Tomography (ERT) allowed us to reveal a complex hypogean cavity system inside the urban area affected by sinkhole since the 1993 (Delle Rose and Leucci, 2010). Here we propose ERT and GPR survey carried out in an area (Fig. 3) next to the 1993 sinkhole collapsed that caused the collapsing of three buildings and irreparable damage to various others, which were demolished later.

FIG. 3 – ERT AND GPR SURVEYED AREAS

For ERT measurements a 48-channel Syscal-Pro Resistivity-meter in a multi electrode configuration using a Wenner–Schlumberger array (Loke 2009) was used. This is a hybrid between the Wenner and Schlumberger arrays (Pazdirek and Blaha 1996) arising out of more recent work with electrical imaging surveys. This array is moderately sensitive to both horizontal and vertical structures. In areas where both types of structures are expected, this array might be a good compromise between the Wenner and the dipole–dipole array (Loke 2009).

GPR measurements were performed using a georadar Ris Hi Mod with a 600 MHz (centre frequency) antenna manufactured by Ingegneria dei Sistemi (IDS).

V. 2D ERT MEASUREMENTS

The 48 electrodes were located on the road surface and spaced 5 m. The line were oriented predominantly in a W-E direction. The measurements were stacked at least three times for each point along the profile to enhance data quality. Standard deviation was used for evaluating the statistical dispersion of recorded resistivity data from their arithmetic mean. The chosen electrode array and spacing made it possible to investigate about 30 m of subsoil with a good resolution. Resistivity data were inverted with the TomoLab software (Geostudi Astier, 2010). The 2D resistivity model is shown in figure 4. It shows the resistivity distribution of the upper 30 m, in which it is possible to note the following: (i) a layer of relatively low resistivity (about 50 ohm m), from the surface to about 2 m in depth (labeled A); (ii) a layer (labeled B) in which resistivity values range between 100 and 150 ohm m; (iii) the area of highest resistivity (ρ = 200 ohm m), inside the layer B; iv) a

deeper layer (labeled C) in which resistivity values range between 100 and 130 ohm m. The model established by means of 2D resistivity imaging profiles thus allows three different zones to be detected and analysed. The first one (A) may correspond to the anthropogenic layer (paving; artificial landfills) in which a groundwater with salt water intrusion is present. The second one (B) corresponds to lamp strata of the laminated and cross-stratified calcarenites and the third one (C) to the moderately cemented massive calcarenites.

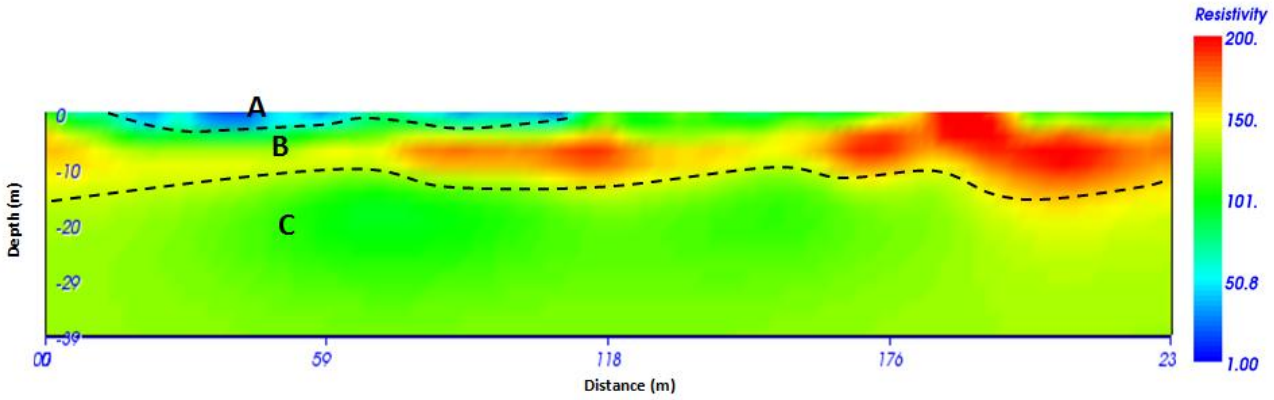

FIG. 4– 2D ERT PROFILE: RESISTIVITY DISTRIBUTION IN THE SUBSOIL

The area of highest resistivity inside the layer B could be related to karstic forms. The location of such a forms well fits a complex marsh depression (probably a group of coalescent dolines or sinkholes) buried below the anthropogenic layer that was detected by means of photo analysis of aerial photo taken before urbanization (Delle Rose and Fiorito, 2000, Fig. 1 of p. 76).

VI. 3D ERT MEASUREMENTS

Twenty ERT lines were acquired at the site over an area of 45×45m^2. The electrode spacing was of 1 m. The ERT line spacing was irregular due to the presence of several buildings. A total of 25500 data points were measured. To avoid damage to the road surface, electrocardiogram electrodes were used. As demonstrated by Leucci (2006, 2007), the electrical resistance contact (ERC) value was of about 2.0 kΩ. As affirmed by Zonge and Hughes (1985), the results were unaffected by this ERC value. The voltage value was set at max voltage, while the injected current values were automatically adjusted by the recording system. Then the measurements were stacked at least three times for each point along the profile to enhance data quality. Standard deviation was used for evaluating the statistical dispersion of recorded resistivity data from their arithmetic mean.

The acquired data were combined to produce three dimensional volumes of the resistivity distribution in the subsoil. The ErtLab software manufactured by Multi-Phase Technologies, LLC, was used to automatically invert the resistivity acquired data and to yield a 3D rho model. Its numerical core based on tetrahedral FEM and inversion was performed with a robust inversion (data variance iterative reweighting). (Geostudi Astier, 2010). The results of the inversion of the electrical data set are shown in Fig 5a and b.

It shows the resistivity distribution in which it is possible to note the following: (i) a layer of relatively low resistivity (about 40–50 ohm m), at depth from the surface ranging from 2m to 3m in depth (labelled A); (ii) a layer (labelled B) in which resistivity values range between 100 and 110 ohm m; (iii) a deeper layer (labeled C) in which resistivity values range between 70 and 80 ohm m; iv) the area of highest resistivity (ρ = 200 ohm m) labeled D. The model established by means of 3D resistivity imaging profiles thus allows three different zones to be detected and analysed. The three zones are similar to those described in the 2D ERT profile analysis. Also here the area of highest resistivity could be related to karstic forms. Particularly the zone labeled "V" could be related to a developed void zone.

The 3D images of resistivity can easily be visualized by 3D contouring of iso-resistivity volumes (Fig. 6). In this representation, the transparency function is defined by two threshold values of the rho, rho1 and rho2 (rho1 < rho2). In the intervals rho < rho1 and rho > rho2, data are rendered as transparent, therefore only the data in the interval rho1 < rho < rho2 are visualized. The threshold calibration is a very delicate task. In fact, by lowering the threshold value, not only the visibility of the main anomaly is raised, but also that of the smaller objects and noise increases. In Fig. 6, the Ip data set is displayed

with iso-IP volumes using a threshold value ranging from 80 to 200Ωm. The continuous high rho anomaly labeled V is more visible. This kind of visualization allows the anomalies resistivity, already shown in Fig. 5, to be emphasized. It is clear the spatial position of karstik form.

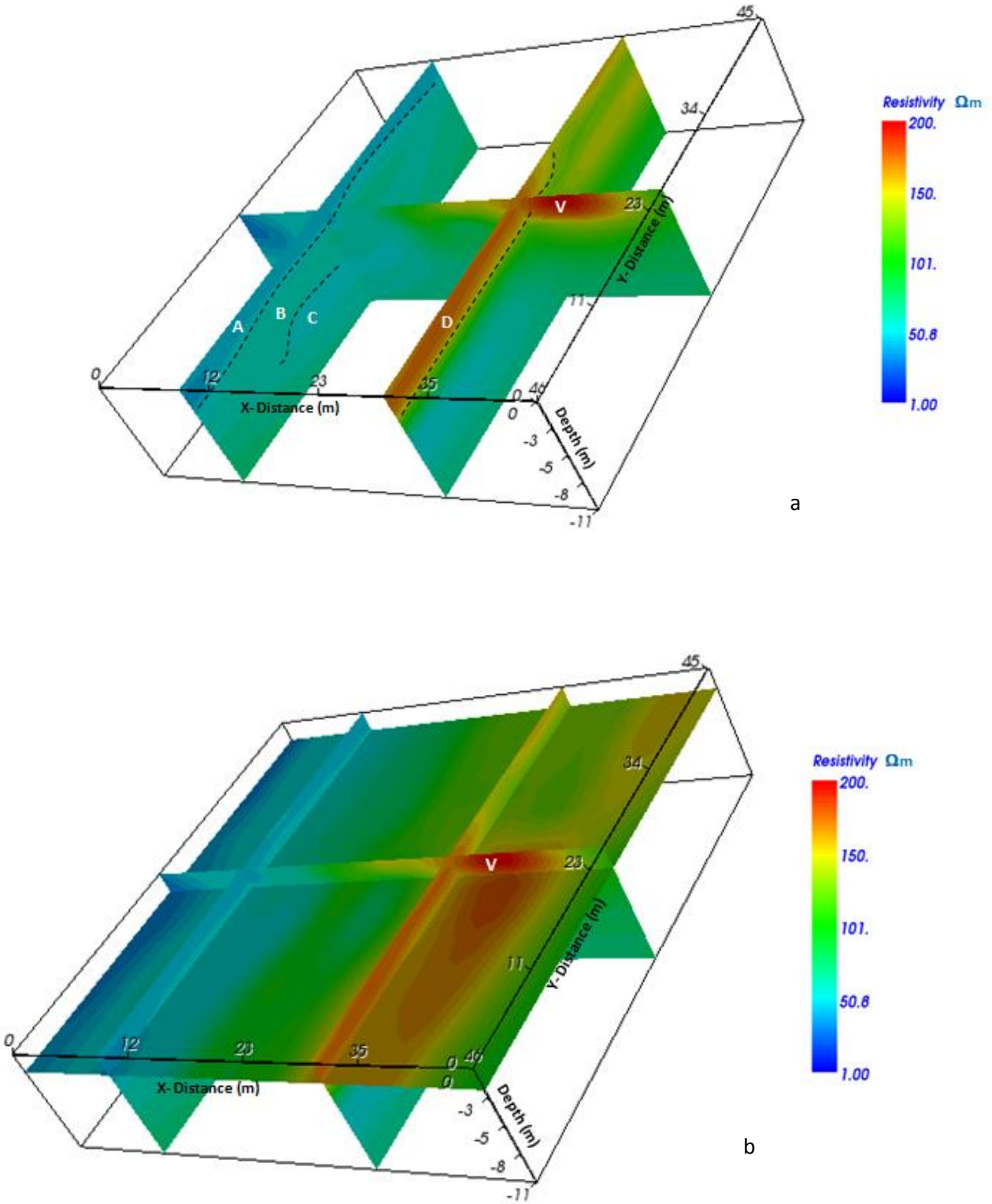

FIG. 5– 3D ERT VOLUME ANALYSIS

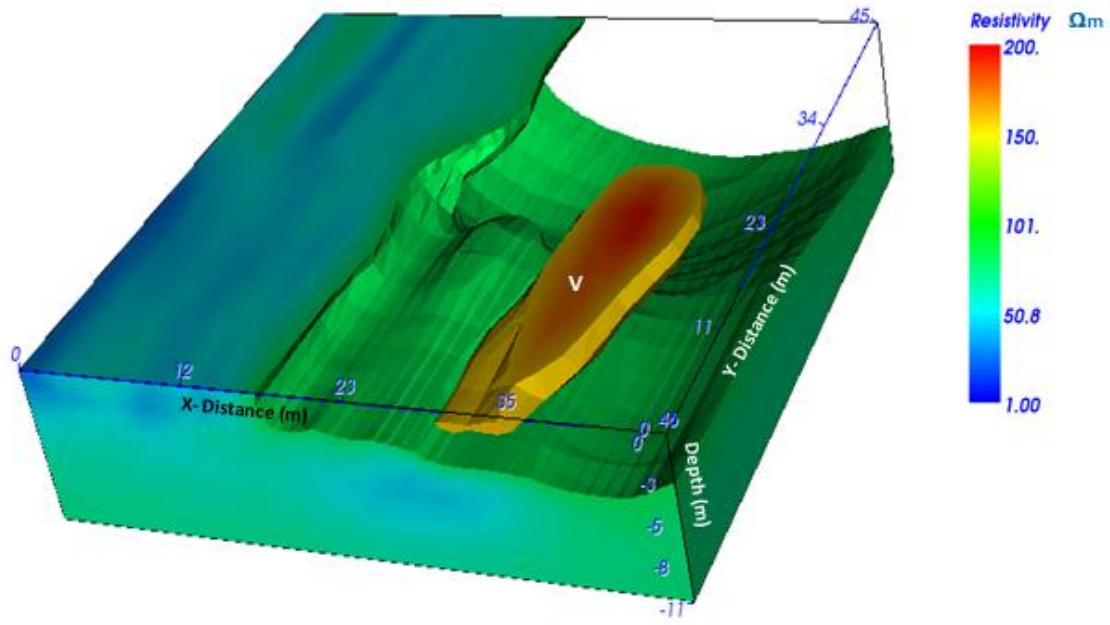

FIG. 6: 3D CONTOURING OF ISO-RESISTIVITY VOLUMES

VII. 3D GPR MEASUREMENTS

A reconnaissance survey was conducted in a continuous mode in an area of 55 m × 12 m. Due to the presence of several buildings, GPR profiles were acquired in a grid with variable dimensions ranging from 0.5m to 1m. The quality of the raw data did not require advanced processing techniques. However, appropriate processing was performed for easier interpretation. The processing steps were a background removal filter process (Conyers and Goodman 1997) and 2D velocity migration (Yilmaz 1987). In order to transform the time axis in depth axis the electromagnetic (EM) wave velocity was esteemated in the surveyed area. EM wave velocity can be estimated from GPR data in several ways; the conventional method involves common depth-point (CDP) and wide-angle reflection and refraction (WARR) data sets. Both methods require two antennas in separate units and relatively long acquisition times. In the first case, both antennas are simultaneously moved apart on either side of the mid-point of

the profile. In the second case, one antenna remains stationary while the other is moved along the profile direction. The EM wave velocity can be more quickly and easily determined from the reflection profiles acquired in a continuous mode, using the characteristic hyperbolic shape of reflection from a

point source (diffraction hyperbola). This is a very common method for the EM velocity estimation and is based on the phenomenon that a small object (the dimensions of the object are smaller than the wavelength of the EM wave introduced in the ground) reflects EM waves in almost every direction.

This method is supported by most radar software packages and should be applied if the diffraction hyperbola occurs at least in 20 radar scans (Fruhwirth and Schmoller 1996). In the data acquired several hyperbolic reflections (Fig. 7), which allow an accurate velocity analysis, are present. The velocity analysis was performed using the GPR-Slice software (Goodman, 2013), on the radar data set, and the application of this method points out an average EM wave propagation velocity of 0.07 m ns^{-1}. Figure 7 shows one of the profiles acquired after the above described processing. A general characteristic of the surveyed area seems to allow a good penetration of electromagnetic (EM) energy (about 60 ns corresponding to a depth of about 2.1 m if the mean velocity value of 0.07 m ns−1 is used). This is essentially due to the physical characteristics of the subsurface, made up of material which poorly dissipates EM energy. This is also the case in all the other profiles acquired in an area.

In the processed radar sections, several reflection events are clearly identifiable. At times ranging from about 20 ns to about 40 ns (0.7 m to 1.4 m in depth) it is possible to identify some reflection events likely due to the probable of karstic forms.

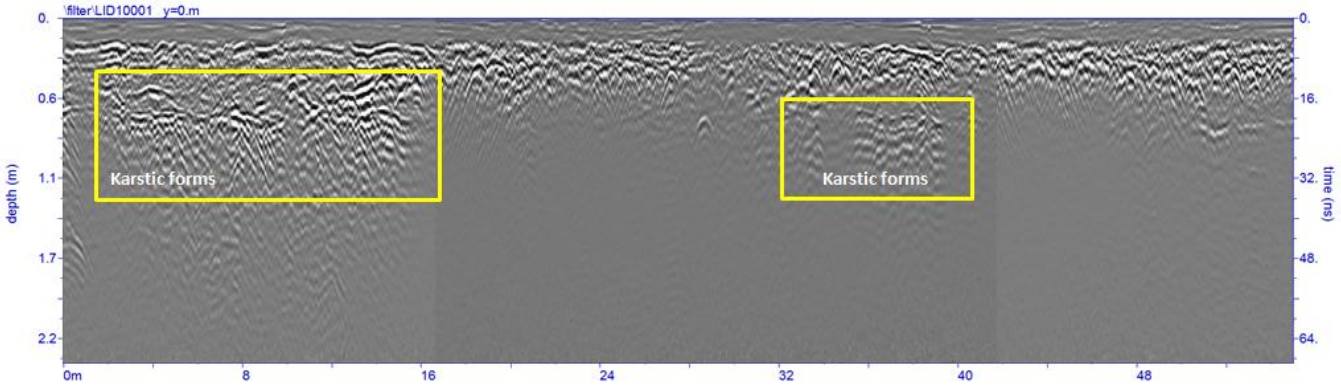

FIG. 7: GPR PROCESSED PROFILE

Since GPR data were acquired in a grid of closely spaced profiles, reflection amplitude can be accurately placed in three dimensions. A way to obtain visually useful maps for understanding the plan distribution of reflection amplitudes within specific time intervals is the creation of horizontal time slices. There are maps on which the reflection amplitudes have been projected at specified time (or depth), with a selected time interval (Conyers, 2006). In a graphic method developed by Goodman et al., (2006), named "overlay analysis", the strongest and weakest reflectors at the depth of each slice are assigned specific colors. This technique allows the linkage of structures buried at different depths. This represents an improvement in imaging because subtle features that are indistinguishable on radargrams can be seen and interpreted in an easier manner. In the present work the time slice technique has been used to display the amplitude variations within consecutive time windows of width $\Delta t = 5$ ns. The time slices (Fig. 8) show the normalized amplitude using a range that define the blue color as the zero level and red color as 1 level. Fig. 8 shows the most significant slices. In the slices ranging from 0.7m to 1.36m depth, relatively high amplitude anomalies are clearly visible in the dashed dark box. These correspond to the karstic forms areas. Moreover the highest amplitudes were rendered into an isosurface (Conyers, 2004, Conyers, 2012, Conyers et al., 2013). 3D amplitude isosurface rendering displays amplitudes of equal value in the GPR study volume. Shading is usually used to illuminate these surfaces, giving the appearance of real archaeological structures. In this case the threshold calibration is a very delicate task in order to obtain useful results.

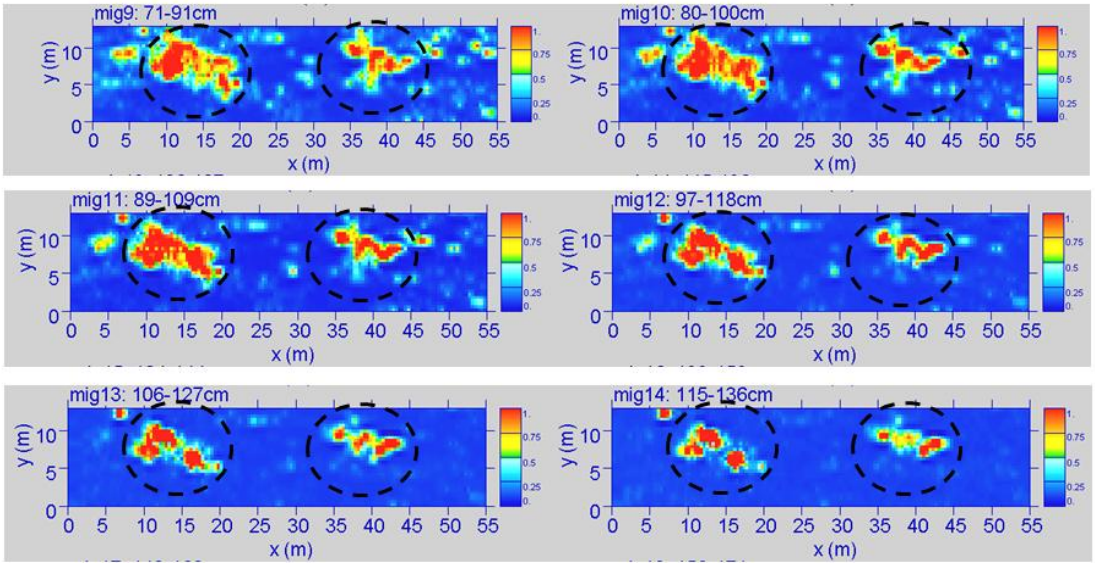

FIG. 8: GPR DEPTH SLICES

This visualization technique better evidence the anomalies found in the surveyed area. In this case is clearly visible the 3D development of the anomalies related to the karstic forms (Fig. 9).

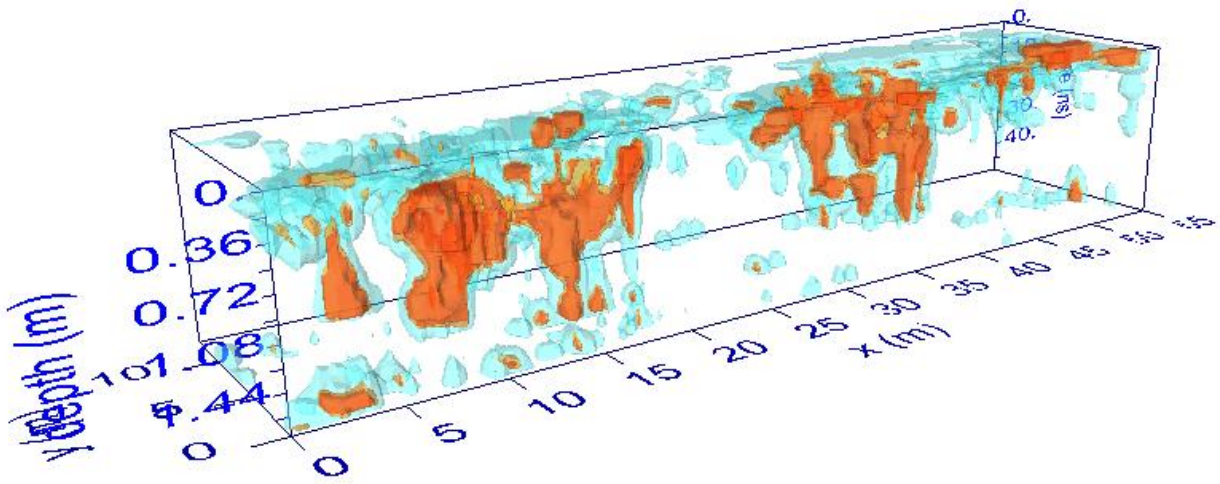

FIG. 9: GPR DATA 3D VISUALIZATION BY THE EM WAVE AMPLITUDE ISO-SURFACE

VIII. HOW GEOLOGICAL UNCERTAINTIES WORSEN THE HAZARD ASSESSMENT

How previous said, three geological-geophysical models were proposed to explain the instability of the underground of Casalabate (Delle Rose and Leucci, 2010; Calò et al., 2011; Margiotta et al., 2012). The first of these considers a shallow karst cavities system in carbonate rocks filled by different kind of deposits (marsh deposits; residual soils; organic soils; sands of beach) suitable to be removed by water flows. In such a context, sinkholes could be due to both the break of cavities' vault (i.e. collapse sinkhole, cf. Waltham et al. 2005) and the down-washing of the filling deposits inside the cavities system (i.e. suffosion sinkhole, cf. Waltham et al. 2005). This latter phenomena "is particularly probable taking into account both the sea level changes and the variations of the piezometric level of the groundwater inside the hypogean system, that can lead high energy water flows that are able to remove and wash away the sediment filling" (Delle Rose and Leucci, 2010, p. 153). According to Calò et al. (2011) the sinkhole "phenomena cannot be due to the collapse of the underground cavities vault, but because of the incidence and combination of the following factors: poor, and in some cases, very poor geotechnical characteristics of foundation grounds; the lack of a preliminary geotechnical characterization of buildings leading to the choice of improper practice in laying down foundations; the letting of rainwater into the subsoil which caused the leaching and the removal of the fine fraction of the foundation grounds". Finally, Margiotta et al. (2012) claim the occurrence of collapse sinkholes inside the marsh deposits and suffosion sinkholes moving down sandy beach deposits. Such these Authors emphasize how their "data" with "particular regard to the stratigraphical succession, are in strong disagreement" with the model of Delle Rose and Leucci (2010) whereas in the same time they are suitable to "mapping the susceptibility to sinkhole" at Casalabate. So, apparently these three models are incompatible each with another one. Really the divergences are mainly due to the different methods to achieve the scientific knowledge or, in other words, they concern epistemological aspects of the research.

Both the models proposed by Delle Rose and Leucci (2010) and Calò et al. (2011) used a stratigraphy reconstruction based the boreholes drilled in the aforementioned project "actions to protect the soil in the hydrogeological risk areas". However, "outcrops available to geological observations are scarce in the Casalabate area, so a borehole survey and sampling had been the key tools to reconstruct the main features of the local geological substratum" (Delle Rose and Leucci, 2010). The subsoil detection performed let us to recognize in the first ten meters of the bedrock two overlap units, the lower of which is a moderately cemented massive calcarenite and the upper unit is formed by sets of variably cemented thinly laminated and cross-stratified calcarenite. As regard the differences between the model proposed by Delle Rose and Leucci (2010) and Calò et al. (2011), these last Authors stressed how "the integrated analysis of information obtained from logs and georadar investigation evidences that […] no cavities and/or channels referable to parakarstic dissolution phenomena have been detected". We point out that only 2 out of 23 boreholes performed on 2008 were performed within the area really affected by sinkholes (the "collapsed area" evidenced in Fig. 3a). Moreover, one of the such two boreholes crossed red residual soils that

are a typical filling of dolines. So, in our opinion, the conclusion of Calò et al. (2011) can be relevant at the entire urban scale but is inconsistent with the scale of the dangerous area. As before said such an area where sinkholes occurred is narrow (about 250 m long and 100 m wide) and close to the coast. However we have to observe that Calò et al. (2011) did not show the profiles of their georadar investigation and therefore don't allow a critical evaluation of their measures and data.

The divergences between the models of Delle Rose and Leucci (2010) and Margiotta et al. (2012) might be explained from the different results of the respective stratigraphy and geophysical surveys. It must be observed that Margiotta et al. (2012) ignored both the aforementioned borehole survey performed on 2008 and the paper of Calò et al. (2011). However they misunderstand the model of Delle Rose and Leucci (2010) especially when they assert that such a model "is based on a stratigraphy consisting exclusively of carbonate deposits, without taking into the due account the crucial presence of cover deposits above the calcarenite bedrock, and primarily that of the organic-rich clays [i.e. marsh deposits]" (Margiotta et al., 2012, p. 667).

Margiotta et al. (2012) described the marsh deposits with a thickness of up to 11 m and overlying (without interruptions) the calcarenites along the coast for an outcropping area ranging from 100 to 250 meters. This stratigraphy setting does not fit the boreholes data of the aforementioned project funded by the Ministry of Environment and Protection of Land: in fact only 6 perforations out of 23 crossed palustrine deposits of thicknesses ranging from 0.3 to 1.4 m. Moreover, the whole stratigraphical model proposed in Margiotta et al. (2012) appears based on subjective considerations. The Authors affirmed that their "research involved […] the critical revision of more than 40 well-core stratigraphies", without describing the nature of such a "critical revision". Their subsoil model seems mainly based on interpretation of geophysical data. Consequently the controversy between the models embraced also methodological aspects regarding data processing and interpretation. We have to observe that for geophysical data Margiotta et al. (2012) associate individual radar signal reflections to specific geological boundaries and even associate a radar signal reflection to a prediction of subsidence. However, it is common practice to perform the radar profiles in correspondence of stratigraphical columns or trenches to be able to associate specific radar reflections to geological stratigraphy (Conyers and Goodman, 1997; Conyers, 2004). A closer look at the geophysical data of Margiotta et al. (2012) is really difficult because the figures were not possible to read the metric scales, time scales, and resistivity scales. Their radar sections are surely affected by ringing (Conyers and Goodman, 1997; Conyers, 2004) probably related to low penetration of radar signal. Seems that the radar signal do not propagate below 20ns. This is due to the high conductive materials presents in the subsoil as confirmed by ERT results presented by the same Authors. In fact in the surveyed area electrical resistivity seems to ranging from 0.5 to 20 ohm m, index of highly conductive subsurface. Therefore the anomalous zones below 20 ns could probably be an artifact due to the application of the background removal filter. For ERT profiles Margiotta et al. (2012) associate resistivity values to specific geological formations. For example 0.5–2 ohm m was related to clay sediments without any reference to a nearby stratigraphycal core or a bibliography. In fact Reynolds, (2011) on page 291, presented a table in which he correlates various types of geological materials with a range of values of electrical resistivity (for clay materials resistivity value ranges from 1 to 150 ohm m). Also in Loke (2011, page 6) for clay materials, resistivity value ranges from 1 to 100 ohm m, while for the sea water resistivity value is about 0.2 ohm□ □ m (due to the relatively high salt content).Given the above, the stratigraphical features of the marsh deposits described by Margiotta et al. (2012) appear inconsistent and the result of a wrong interpretation of geophysical data. Consequently, their model of sinkhole susceptibility is questionable.

IX. CONCLUSION

The case of Casalabate is a good example of how geological uncertainties can worsen the hazard assessment. In consideration of the complexity of the problem and the concerns of the collectivity, an efficient predictive model of the hazard should be defined. In order to select the most appropriate geological-geophysical model, confrontations among all the researchers working on this issue would be desirable. Especially the knowledge exchange between geologists and geophysicists must be improved. As revealed the ERT and GPR surveys exposed in this paper, dangerous cavities could be placed also out of the area repeatedly interested by sinkholes since 1993. Consequently an efficient predictive model taking into account the hydrogeology and hydraulic context, especially the occurrence of rains and sea storms, must be produced.

REFERENCES

[1] Anderson, M.P. and Woessner W.W.; 1992: Applied Groundwater Modeling. Academic Press, Inc., San Diego, 381 pp.

[2] Calò P., Macrì F., Piccinni F. and Tinelli R.; 2011: Instabilità del centro urbano di Casalabate (Lecce, italia): analisi delle condizioni di rischio - Instability of Casalabate village (Lecce, Italy): analisys of risk conditions. Italian Journal of Engineering Geology and Environment, 11(1), 55-64.

[3] Conyers L.B. and Goodman D.; 1997: Ground-penetrating radar – an introduction for archaeologists. Alta Mira Press.

[4] Conyers L.B.; 2004: Ground-Penetrating Radar for Archaeology. (Walnut Creek, CA: Alta Mira).

[5] Conyers L.B. 2006. Innovative ground-penetrating radar methods for archaeological mapping: Archaeological Prospection, v. 13, no. 2, p. 139-141.

[6] Conyers L.B., 2012. Interpreting Ground-penetrating Radar for Archaeology. Left Coast Press: Walnut Creek, CA.

[7] Conyers L.B., Daniels J.M., Haws J., Benedetti M., 2013. An Upper Palaeolithic Landscape Analysis of Coastal Portugal Using Ground-penetrating Radar. Archeologica Prospettino, 20, 45-51;

[8] Delle Rose M. and Fiorito F.; 2000: Ipotesi di recupero del territorio di Casalabate. Economia e Società, 2, 71-81.

[9] Delle Rose M. and Federico A.; 2002: Karstic phenomena and environmental hazard is Salento costal plains. Proc. IX IAEG Congress, J.L. van Rooy and C.A. Jermy editors, Durban, 1297-1305.

[10] Delle Rose M. and Leucci G.; 2010: Towards an integrated approach for characterisation of sinkhole hazards in urban environments: the unstable coast site of Casalabate, (Lecce, Italy). Journal of Geophysics and Engineering, 7, 143-154.

[11] Leucci G 2006 Contribution of ground penetrating radar and electrical resistivity tomography to identify the cavity and fractures under the main Church in Botrugno (Lecce, Italy) J. Archaeol. Sci. 33 1194–204

[12] Leucci G 2007 Geoscientific investigations for mapping the subsidence risk in an urban area J. Geophys. Eng. 4 317–31

[13] Fruhwirth R K and Schmoller R 1996 Some aspects on the estimation of electromagnetic wave velocities Proc. of the 6th Int. Conf. on Ground Penetrating Radar (GPR '96), (Sendai, Japan, 30 September–3 October 1996) pp 135–8

[14] Geostudi Astier; 2010: ErtLab Solver – Release 1.3.1.

[15] Goodman D., 2013. GPR Slice v 7.0 Manual. From http://www.gpr-survey.com June, 2013

[16] Goodman D., Steinberg J., Damiata B., Nishimure Y., Schneider K., Hiromichi H., Hisashi N., 2006. Gpr Overlay Analysis for Archaeological Prospection, Proceedings of the 11th International Conference on Ground Penetrating Radar, Columbus, Ohio USA. CD-rom

[17] Loke M.H.; 2011: Tutorial: 2-D and 3-D electrical imaging surveys. www.geoelectrical.com

[18] Margiotta S., Negri S., Parise M. and Valloni R.; 2012: Mapping the susceptibility to sinkholes in coastal areas, based on stratigraphy, geomorphology and geophysics. Nat. Hazards, 62, 657–676.

[19] Pazdirek O. and Blaha V.; 1996: Examples of resistivity imaging using ME-100 resistivity field acquisition system. EAGE 58th Conf. and Technical Exhibition Extended Abstracts, Amsterdam.

[20] Reynolds J.M.; 2011: An Introduction to Applied and Environmental Geophysics, John Wiley & Sons Ltd., Baffins Lane, Chichester, second edition.

[21] Rossi D.; 1969: Note illustrative della Carta Geologica d'Italia. Fogli 203, 204, 213 – Brindisi, Lecce, Maruggio. Servizio Geol. It., 42 pp.

[22] Zonge K L and Hughes L J 1985 The effect of electrode contact resistance on electric field measurements Proc. 55th Annual SEG Convention (Washington, DC, 6–10 October 1985)

[23] Yilmaz O 1987 Seismic Data Processing ed E B Neitzel (Tulsa, OK: Society of Exploration Geophysicists)